Polarization aberrations. I. Rotationally symmetric optical systems

James P. McGuire, Jr.
Russell A. Chipman

May 21, 1990

1 Introduction

The analysis of the polarization characteristics displayed by optical systems can be divided into two categories: geometrical and physical. Geometrical analysis calculates the change in polarization of a wavefront between pupils in an optical instrument [1,2,3,4]. Physical analysis propagates the polarized fields wherever the geometrical analysis is not valid, i.e. near the edges of stops, near images, in anisotropic media, etc. [1,5,6,7,8]. The changes, geometrical and physical, polarization causes in the performance of lens and mirror systems are readily calculated by several commercial computer codes [9,10,11,12]. The inverse problem of designing a system with specified polarization characteristics is more difficult. Examples in the literature include a polarization compensated polarizing microscope[13] and a telescope with ultra-low polarization for a solar polarimeter [14]. Design requires a fundamental understanding of the origin of polarization aberrations and how they change with both the optical and coating prescriptions for a system. Polarization aberration theory provides a starting point for geometrical design and facilitates subsequent optimization.

Chipman has derived several polarization aberration expansions similar to the classical wavefront expansion for rotationally symmetric systems valid for *weak* second order aberrations [15,16,2]. Reference [17] explores polarization aberrations graphically using a "symmetrized" second order expansion valid for *strong* aberrations but does not describe a method to calculate the aberration coefficients. In this paper, we calculate and discuss an exponential expansion of the polarization aberrations valid for *strong* polarization aberrations through fourth order[1]. The results are applied to the interpretation of polarization raytracing results.

The polarization aberrations described in this paper arise from differences in the transmitted (or reflected) amplitudes and phases at interfaces. In contrast, classical wavefront aberrations arise from differences in optical path length as rays propagate between interfaces [18]. Figure 1 shows the calculation of the optical path length W and the optical path length *and* the polarization $\mathbf{J}$ along a ray. Repetition of the calculation depicted in Figure 1 (a) for multiple rays and wavelengths samples the wavefront aberration function. Repetition of the calculation 1 (b) for multiple rays and wavelengths samples the wavefront aberration function and the polarization aberration matrix (PAM) of the system. The PAM describes the variation in polarization with object coordin pupil coordinates, and wavelength. This paper calculates the PAM for isotropic rotationally symmetric systems through fourth order and includes the interface phase, amplitude, linear diattenuation (defined in Table 1), and linear retardance aberrations. Polarization aberrations resulting from propagation through anisotropic media such as crystals are not considered in this paper. For propagation through anisotropic crystals, the propagation terms $\exp[jW_{nm}]$ in Figure 1 (b) would be replaced by Jones matrices $\mathbf{J}_{nm}$.

The order of an aberration term referred to in this paper is the order of the wavefront representation (n), not the order of the transverse aberrations ($n-1$). Thus, defocus and tilt are second order aberrations, while spherical aberration, coma, and astigmatism are fourth order aberrations (not third order aberrations).

Section 2 discusses the exponential form of Jones matrices used in this paper. Section 3 introduces the PAM in Jones matrix form. In Section 4, the exact calculation of polarization aberrations through polarization raytracing is described. Section 5 presents the coordinate system used in this paper. Section 6 discusses the paraxial approximation including: the paraxial PAM for a single surface, paraxial angle of incidence, and the paraxial orientation of the plane of incidence. In Section 7, a Taylor series simplifies coating dependence of the single surface paraxial

[1] The preliminary version of this paper used did not use the exponential form which resulted in increased complexity of computation and interpretation.

Table 1: Polarization terminology

Term	Definition
Diattenuation	The property of having an intensity transmittance which is dependent on the incident polarization state.
Polarization	The property of altering the polarization state of light. Polarization includes the subsets of diattenuation and retardance.
Polarizer	An optical element which transmits a fixed polarization state independent of the incident polarization state. Examples include dichroic sheets (Polaroid) and Glan-Thompson prisms.
Polarization element	Any optical element showing polarization. Examples include retarders, polarizers, and metallic interfaces.
Retardance	The property of having a phase or optical path length which is dependent on the incident polarization state.

Note: There is a distinction between polarizer and polarization element. Chipman provides a more detailed discussion [2].

PAM. Section 8 calculates the paraxial PAM for a system of isotropic rotationally symmetric elements through fourth order. A general discussion of the terms is contained in Section 9. Section 10 contains a detailed discussion of the vector aberrations (defined later) comparing and contrasting them with classical scalar phase aberrations. Section 11 discusses interpretation of polarization raytracing in the context of the aberration theory results. Appendix A contains paraxial expressions for polarization basis vectors. Appendix B examines the polarization by uncoated interfaces. Appendix C lists the polarization aberration coefficients for a system of isotropic rotationally symmetric elements.

2 Jones Matrices

In this section, we present the Jones matrix formalism[19,20] for the analysis of polarization as used in this paper.

The Jones vector $\vec{U}(t)$ is

$$\vec{U}(t) = \begin{pmatrix} \vec{U}_q(t) \\ \vec{U}_r(t) \end{pmatrix} \tag{1}$$

where $\vec{U}_q(t)$ and $\vec{U}_r(t)$ are the projections of the electromagnetic field on any two orthogonal basis states q and r. The Jones matrix $\mathbf{J}$ relates the incident $\vec{U}$ and transmitted fields $\vec{U}'$

$$\vec{U}' = \mathbf{J}\vec{U} \tag{2}$$

and is a 2x2 matrix with complex elements

$$\mathbf{J} = \begin{pmatrix} j_{11} & j_{12} \\ j_{21} & j_{22} \end{pmatrix} \tag{3}$$

Table 3: Physical significance of the exponential polarization coefficients

Coefficient	Matrix	Physical significance	
a_0	σ_0	$\Re(a_0)$:	Polarization independent amplitude
		$\Im(a_0)$:	Polarization independent phase
a_1	σ_1	$\Re(a_1)$:	Linear diattenuation along the coordinate axes
		$\Im(a_1)$:	Linear retardance along the coordinate axes
a_2	σ_2	$\Re(a_2)$:	Linear diattenuation at 45 degrees to the coordinate axes
		$\Im(a_2)$:	Linear retardance at 45 degrees to the coordinate axes
a_3	σ_3	$\Re(a_3)$:	Circular diattenuation
		$\Im(a_3)$:	Circular retardance

$$\vec{U}_{xp}(\vec{h},\vec{\rho},\lambda) = \mathbf{J}_{sys}(\vec{h},\vec{\rho},\lambda)\vec{U}_{np}(\vec{h},\vec{\rho},\lambda) \tag{5}$$

where the Jones matrix is

$$\begin{aligned}\mathbf{J}_{sys}(\vec{h},\vec{\rho},\lambda) &= \begin{pmatrix} j_{sys,11}(\vec{h},\vec{\rho},\lambda) & j_{sys,12}(\vec{h},\vec{\rho},\lambda) \\ j_{sys,21}(\vec{h},\vec{\rho},\lambda) & j_{sys,22}(\vec{h},\vec{\rho},\lambda) \end{pmatrix} \\ &= \exp[a_{sys,0}\sigma_0 + a_{sys,1}\sigma_1 + a_{sys,2}\sigma_2 + a_{sys,3}\sigma_3] \end{aligned} \tag{6}$$

and $\vec{h}$ is the object coordinate, $\vec{\rho}$ is the pupil coordinate, and λ is the wavelength.

It is convenient to separate the Jones matrix for an imaging system into a polarization aberration matrix (PAM) which describes the aberrations and a "quadratic phase" characteristic of ideal imaging systems

$$\mathbf{J}_{sys}(\vec{h},\vec{\rho},\lambda) = \mathbf{J}(\vec{h},\vec{\rho},\lambda)\exp\left[\frac{-jk\vec{\rho}\cdot\vec{\rho}}{2f}\right] \tag{7}$$

where $\mathbf{J}(\vec{h},\vec{\rho},\lambda)$ is the PAM, f is focal length, and $k = 2\pi/\lambda$ is the wavenumber. Both the wavefront aberrations and the finite extent of lens are described by the elements of $\mathbf{J}$ (the finite size of the lens is an "aberration" which reduces resolution from that predicted by geometrical optics.) In the limit of a non-polarizing optical system, the PAM has the form

$$\mathbf{J}(\vec{h},\vec{\rho},\lambda) = P(\vec{h},\vec{\rho})\exp\left[jkW(\vec{h},\vec{\rho},\lambda)\right]\begin{pmatrix} 1 & 0 \\ 0 & 1 \end{pmatrix} \tag{8}$$

where $P(\vec{h},\vec{\rho})$ is the pupil function which describes the amplitude transmittance of the pupil and $W(\vec{h},\vec{\rho},\lambda)$ is the wavefront aberration function. In succeeding sections, quasi-monochromatic light is assumed and the explicit wavelength dependence λ is suppressed.

4 Exact Polarization Raytracing

In this section, we describe the procedure for calculating the change in polarization along a ray through a system of isotropic surfaces. The technique is called polarization raytracing [23,24].

$$\begin{aligned} \mathbf{J}_q(i_q, \theta_q) &= \mathbf{J}_q(i_q)\mathbf{R}(\theta_q) \\ &= \begin{pmatrix} a_{sq}(i_q)\cos\theta_q & a_{sq}(i_q)\sin\theta_q \\ -a_{pq}(i_q)\sin\theta_q & a_{pq}(i_q)\cos\theta_q \end{pmatrix} . \end{aligned} \tag{19}$$

Equation (19) is exact Jones matrix for an isotropic interface. Isotropic interfaces do not display circular polarization or circular retardance. If a ray $\hat{R}_1$ is incident on a system of surfaces, the polarization along $\hat{R}_1$ is found by cascading the effects from each surface

$$\mathbf{J}(\hat{R}_1) = \prod_{q=Q}^{1} \mathbf{J}_q(i_q, \theta_q) \ . \tag{20}$$

The set of all Jones matrices for a system for each possible ray path $\hat{R}_1$ and wavelength is the PAM, as described in Section 3. Polarization raytracing codes [10,11,12] sample the PAM by calculating (20) for selected rays and wavelengths. Reference [9] uses Mueller matrices to sample polarization aberrations. The rest of this paper examines a fourth order approximation to the PAM for rotationally symmetric systems.

5 Global Coordinates

For polarization aberrations expansions, an object and pupil coordinate system is required. We denote the object height by H and normalize it to one at the edge of the field of view. The object is located along the global y-axis without loss of generality because of the rotational symmetry of the system. The entrance pupil coordinates are denoted by either (x, y, z) or (ρ, ϕ, z) in Cartesian and cylindrical coordinates. In the paraxial approximation the pupils are flat, so the z dependence is dropped for convenience in much of this paper. The pupil coordinates x, y, and ρ are normalized to one at the edge of the entrance pupil. The polar angle ϕ is defined so that

$$x = -\rho\sin\phi \tag{21}$$

$$y = \rho\cos\phi \ . \tag{22}$$

Figure 2 illustrates the normalized coordinate system.

6 Paraxial Polarization Aberration Matrices

In this section, we determine the paraxial PAM for a rotationally symmetric surface. Appendix A provides paraxial expressions for the surface normal and local $(\hat{R}_q, \hat{S}_q, \hat{P}_q)$ basis vectors. The single surface Jones matrix of Section 4 is simplified to first the paraxial Jones matrix and then to the paraxial PAM. The accuracy of the paraxial approximation for the angle of incidence and orientation of the plane of incidence are examined.

Consider the polarization of a ray for a system of surfaces. Because the paraxial fields remain in the x-y plane [see (A-9) and (A-10)], we choose x-y Jones basis vectors at each surface. Then, the Jones matrix for each surface consists of a rotation into s-p coordinates, the Jones matrix in s-p coordinates, and finally a rotation back to the x-y coordinates

dependence of the paraxial PAM is suppressed for notational convenience. The paraxial angle of incidence is obtained by expanding the angle of incidence (17) in a Taylor series

$$\begin{aligned} i_q(H,\rho,\phi) &= \arcsin\left|\vec{S}_q\right| \\ &= \left|\vec{S}_q\right| + \frac{1}{6}\left|\vec{S}_q\right|^3 + \cdots \\ &= \sqrt{H^2 i_{cq}^2 + 2H\rho\cos\phi\, i_{cq} i_{mq} + \rho^2 i_{mq}^2} \end{aligned} \tag{28}$$

where the term linear in object and pupil coordinates was retained. The paraxial orientation of the angle of incidence (24) in terms of $\cos[2\theta_q(H,\rho,\phi)]$ and $\sin[2\theta_q(H,\rho,\phi)]$ is

$$\cos[2\theta_q(H,\rho,\phi)] = \frac{H^2 i_{cq}^2 + 2H\rho\cos\phi\, i_{cq} i_{mq} + \rho^2 i_{mq}^2 \cos 2\phi}{i_q^2} \tag{29}$$

$$\sin[2\theta_q(H,\rho,\phi)] = \frac{-2H\rho\sin\phi\, i_{cq} i_{mq} - \rho^2 i_{mq}^2 \sin 2\phi}{i_q^2} . \tag{30}$$

Equations (28) through (30) define the paraxial system geometry.

Next, consider the accuracy of the paraxial orientation of the plane of incidence and angle of incidence at a spherical interface. The paraxial orientation of the plane of incidence assumes that the $\hat{S}_q$ and $\hat{P}_q$ basis vectors are in the x-y plane. A measure of the accuracy of this approximation is the ratio of the intensity of the field in the x-y plane to the total intensity

$$I_{xy}(\vartheta) = \frac{|U_x|^2 + |U_y|^2}{|U|^2} = \cos^2\vartheta \tag{31}$$

where ϑ is the angle the ray makes with the z-axis. When $I_{xy} \approx 1$, most of the light is polarized in the x-y plane and the paraxial approximation is good. When $I_{xy} \approx 0$, most of the light is polarized in either the x-z or y-z planes and the paraxial approximation is not valid. Now consider the angle of incidence. The surface normal for a sphere from the definition (A-2) is

$$\hat{N} = \left(-\frac{x}{R_l}, -\frac{y}{R_l}, \frac{1}{R_l}\sqrt{R_l^2 - (x^2+y^2)}\right) \tag{32}$$

where R_l is the radius of curvature of the sphere. If the axial plane waves $\hat{R} = (0,0,1)$ are incident then

$$\begin{aligned} i &= \arcsin\left(\frac{\rho}{R_l}\right) \\ &= \frac{\rho}{R_l} + \frac{1}{6}\left(\frac{\rho}{R_l}\right)^3 + \frac{3}{40}\left(\frac{\rho}{R_l}\right)^5 + \cdots \end{aligned} \tag{33}$$

where $\rho = \sqrt{x^2+y^2}$. Figure 3 shows a comparison between several approximations to the angle of incidence for a spherical mirror. The high degree of linearity of the exact curve, even with angles of incidence as large as 30°, permits the paraxial approximation to the geometry to be used for many systems.

$$r'_{a2} = r_{a2}/r_0 \tag{39}$$
$$r'_{a4} = r_{a4}/r_0 - 0.5(r_{a2}/r_0)^2 \ . \tag{40}$$

Finally, substituting the Fresnel expansion coefficients into (25) gives the paraxial PAM expansion

$$\mathbf{J}_q(H,\rho,\phi) = \exp\left\{ \begin{array}{l} (a_{00q} + a_{02q}\, i_q^2 + a_{04q}\, i_q^4 + \ldots)\sigma_0 + \\ (a_{12q}\, i_q^2 + a_{14q}\, i_q^4 + \ldots)(\cos 2\theta_q \sigma_1 + \sin 2\theta_q \sigma_2) \end{array} \right\} \tag{41}$$

where $i_q = i_q(H,\rho,\phi)$ and $\theta_q = \theta_q(H,\rho,\phi)$ are defined in (28) through (30) and the coating coefficients $a_{0,2k,q}$ and $a_{1,2k,q}$ are

$$a_{0,2k,q} = \left[r'_{s,2k,q} + r'_{p,2k,q} + j(\psi_{s,2k,q} + \psi_{p,2k,q})\right]/2 \tag{42}$$
$$a_{1,2k,q} = \left[r'_{s,2k,q} - r'_{p,2k,q} + j(\psi_{s,2k,q} - \psi_{p,2k,q})\right]/2 \ . \tag{43}$$

The subscripts of coefficients $a_{0,2k,q}$ and $a_{1,2k,q}$ are assigned as follows. The first subscript assumes the value 0 for the polarization independent contribution and 1 for the linear polarization along the s-p axis. The second subscript, $2k$, is the order of the coefficient. The last subscript, q, designates surface number.

8 Polarization Aberration Matrices for Systems

In this section, we obtain the paraxial PAM for an optical system of isotropic rotationally symmetric elements through fourth order. Sections 9 and 10 discuss the system PAM.

To begin, we introduce the Baker-Campbell-Hausdorff (BCH) identity [25].

Baker-Campbell-Hausdorff 1 *If* $\mathbf{A}$ *and* $\mathbf{B}$ *are matrices, or certain other non-commuting operators, then*

$$\exp \mathbf{A} \exp \mathbf{B} = \exp\left[\mathbf{A} + \mathbf{B} + \mathbf{C}_2 + \mathbf{C}_3 + \cdots\right] \tag{44}$$

where $\mathbf{C}_k$ *is a linear combination of k-fold commutators of* $\mathbf{A}$ *and* $\mathbf{B}$*, in particular*

$$\mathbf{C}_2 = \frac{1}{2}[\mathbf{A},\mathbf{B}] \tag{45}$$
$$\mathbf{C}_3 = \frac{1}{12}[[\mathbf{A},[\mathbf{A},\mathbf{B}]] - [\mathbf{B},[\mathbf{A},\mathbf{B}]]] \ . \tag{46}$$

The BCH identity consistently carries out operator products, retaining terms to a given order.

Now, the PAM of an optical system with Q surfaces is the product of the PAMs of the individual surfaces

$$\mathbf{J} = \mathbf{J}_Q \mathbf{J}_{Q-1} \cdots \mathbf{J}_2 \mathbf{J}_1 \tag{47}$$

which simplifies to

$$\mathbf{J} = \exp\left[a_0\sigma_0 + a_1\sigma_1 + a_2\sigma_2 + a_3\sigma_3\right] \tag{48}$$

using the paraxial surface PAM (41), the BCH identity, and the commutation relations in Table 4. The system PAM coefficients to fourth order are

$$
\mathrm{J}(H,\rho,\phi) = \exp\left\{\begin{array}{ll}
P_{0000}\sigma_0 + & \text{constant piston}\\
P_{0200}H^2\sigma_0 + & \text{quadratic piston}\\
P_{0111}H\rho\cos\phi\,\sigma_0 + & \text{tilt}\\
P_{0022}\rho^2\sigma_0 + & \text{defocus}\\
P_{0040}\rho^4\sigma_0 + & \text{spherical aberration}\\
P_{0131}H\rho^3\cos\phi\,\sigma_0 + & \text{coma}\\
P_{0222}H^2\rho^2\cos 2\phi\,\sigma_0 + & \text{astigmatism and field curvature}\\
P_{0311}H^3\rho\cos\phi\,\sigma_0 + & \text{distortion}\\
P_{0400}H^4\sigma_0 + & \text{quartic piston}\\
P_{1200}H^2\sigma_1 + & \\
P_{1111}H\rho(\cos\phi\,\sigma_1 - \sin\phi\,\sigma_2) + & \\
P_{1022}\rho^2(\cos 2\phi\,\sigma_1 - \sin 2\phi\,\sigma_2) + & \\
P_{1400}H^4\sigma_1 + & \\
P_{1311}H^3\rho(2\cos\phi\,\sigma_1 - \sin\phi\,\sigma_2) + & \\
P_{1222}H^2\rho^2\cos\phi\,(\cos\phi\,\sigma_1 - \sin\phi\,\sigma_2) + & \\
P_{1133}H\rho^3\cos\phi\,[(1+\cos 2\phi\,)\,\sigma_1 - \sin 2\phi\,\sigma_2] + & \\
P_{1042}\rho^4(\cos 2\phi\,\sigma_1 - \sin 2\phi\,\sigma_2) + & \\
P_{3131}H\rho^3\sin\phi\,\sigma_3 + & \text{circular polarization coma}\\
P_{3311}H^3\rho\sin\phi\,\sigma_3 + & \text{circular polarization distortion}\\
\text{sixth order terms} &
\end{array}\right\} \tag{53}
$$

or in Cartesian coordinates

$$
\mathrm{J}(H,x,y) = \exp\left\{\begin{array}{ll}
P_{0000}\sigma_0 + & \text{constant piston}\\
P_{0200}H^2\sigma_0 + & \text{quadratic piston}\\
P_{0111}Hy\sigma_0 + & \text{tilt}\\
P_{0022}(x^2+y^2)\sigma_0 + & \text{defocus}\\
P_{0040}(x^2+y^2)^2\sigma_0 + & \text{spherical aberration}\\
P_{0131}Hy(x^2+y^2)\sigma_0 + & \text{coma}\\
P_{0222}H^2(y^2-x^2)\sigma_0 + & \text{astigmatism and field curvature}\\
P_{0311}H^3y\sigma_0 + & \text{distortion}\\
P_{0400}H^4\sigma_0 + & \text{quartic piston}\\
P_{1200}H^2\sigma_1 + & \\
P_{1111}H(y\sigma_1 + x\sigma_2) + & \\
P_{1022}\left[(y^2-x^2)\,\sigma_1 + 2xy\sigma_2\right] + & \\
P_{1400}H^4\sigma_1 + & \\
P_{1311}H^3(2y\sigma_1 + x\sigma_2) + & \\
P_{1222}H^2y\,(y\sigma_1 + x\sigma_2) + & \\
P_{1133}Hy\left[(1+y^2-x^2)\,\sigma_1 + 2xy\sigma_2\right] + & \\
P_{1042}\left[(y^4-x^4)\,\sigma_1 + 2xy\,(x^2+y^2)\,\sigma_2\right] + & \\
P_{3131}Hx\,(x^2+y^2)\,\sigma_3 + & \text{circular polarization coma}\\
P_{3311}H^3x\sigma_3 + & \text{circular polarization distortion}\\
\text{sixth order terms} &
\end{array}\right\} \tag{54}
$$

where the terms are grouped based on their H, ρ, ϕ dependencies and P_{tuvw} are the polarization aberration coefficients. The polarization aberration coefficients are sums over interface contributions as given in Appendix C and assigned subscripts using the convention: t denotes the type of polarization behavior[2], u denotes the order of the H dependence, v denotes the order of the ρ dependence, and w denotes the order of the ϕ dependence.

The fourth order paraxial PAM is paraxial in system geometry and fourth order in coating response to changes in angle of incidence. A subtle consequence is that

thin film coatings (particularly those with many layers), they can be significant. Our equations only calculate the system wavefront aberration contributions arising from coatings. The geometrical portion of the classical wavefront aberrations (those arising from optical path length differences) are calculated by the paraxial ray trace and conventional aberration calculations [18].

The second class of aberrations contains the *amplitude or apodisation aberrations* which are characterized by the real parts of the σ_0 coefficients, $\Re(P_{0uvwx})$. The amplitude aberrations are variations of the amplitude of the electromagnetic field across the exit pupil which are independent of the incident polarization state. They do not describe the shape of the transmitted wavefront, only its amplitude. This apodisation is due to the optical system, not to intensity variations in the incident light, such as the Gaussian profile of a laser beam. The amplitude aberrations describe the average of the coating amplitude transmittance of the s and p light (the polarization terms describe the difference). Amplitude aberrations are scalar aberrations and have the same functional dependence on object and pupil coordinates as the classical wavefront aberrations. Contours of constant apodisation aberrations through fourth order are shown in Figure 4. Since the functional form is the same, the generic names of the functions have been retained with the prefix amplitude added: amplitude tilt, amplitude coma, amplitude spherical aberration, etc. For example, the term $\Re(P_{0040})\rho^4$ is amplitude spherical aberration. If $\Re(P_{0040})$ is negative the center of the pupil is brighter and the pupil becomes dimmer quartically with pupil radius. For $\Re(P_{0uvwx})$ positive, the pupil is brighter at the edge. The interpretation of all of the amplitude aberration follows in the same manner as amplitude spherical aberration. Intentional apodisation (versus apodisation aberrations) is discussed in Reference [26].

The third and fourth classes of aberrations contain linear diattenuation and linear retardance aberrations and are characterized by the real and imaginary parts of the coefficients of σ_1 and σ_2 respectively. These two classes of aberrations are characterized by the real and imaginary parts of the coefficients of σ_1 and σ_2 respectively. These two classes of aberration will be treated together under the name *vector aberrations*. Vector aberrations are conceptually different from the scalar aberrations since both a magnitude and orientation must be specified. The paraxial vector aberration patterns through fourth order are illustrated in Figure 5. The length of the lines denotes the strength of the linear polarization element. The orientation of the line denotes the orientation of the linear polarization element. The patterns are the same for both linear diattenuation and linear retardance aberrations since both are vector aberrations. A detailed discussion of the vector aberrations is found in the next section.

The effect of the vector polarization aberrations on polarized incident light is the same as a linear polarization element with spatially varying strength and orientation. Figures 6 and 7 show the effect of the three second order aberrations on linearly polarized light. The magnitudes of the aberrations depicted are not typical, but have been chosen to clearly display the effect of the aberrations. Figures 8 and 9 depict the effect of the three second order aberrations on circularly polarized light. The type and orientation of ellipse indicates the type and orientation of the polarization state. The position and direction of the arrow denotes phase and handedness of the polarization state.

The last class of aberrations contain the *circular aberrations*. Figure 4 shows contours of constant circular aberrations through fourth order. The real and imaginary parts of the coefficient of σ_3 correspond to the circular diattenuation and circular retardance aberrations respectively. The circular aberrations are variations of the circular diattenuation and circular retardance across the exit pupil. The imaginary part of the term P_{3131} [P_{3311}] produces a wavefront with $\Im(P_{3131})$ coma [$\Im(P_{3311})$ distortion] when right circularly polarized light is incident and $-\Im(P_{3131})$ coma

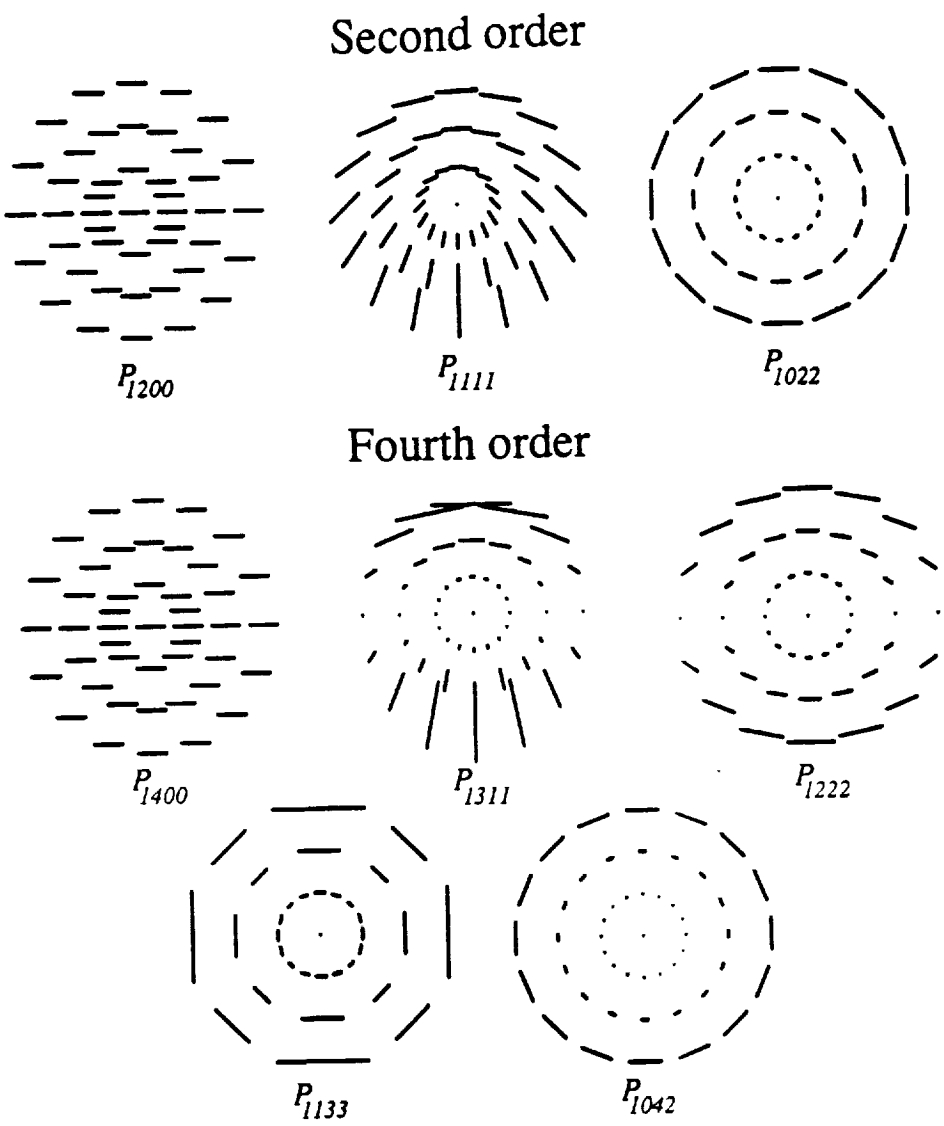

Figure 5: Paraxial vector polarization aberration patterns through fourth order

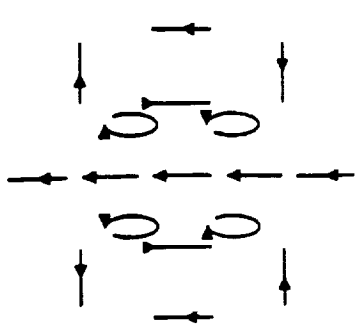

Linearly polarized light incident
(a)

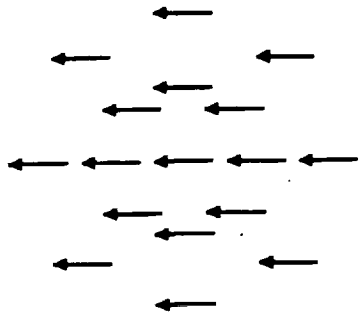

$P_{1022} = j\pi/2$
(b)

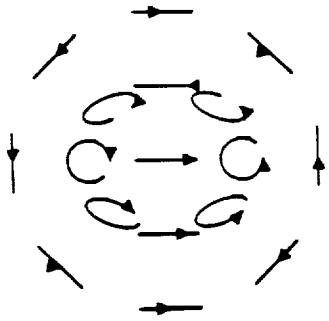

$P_{1111} = j\pi/2$
(c)

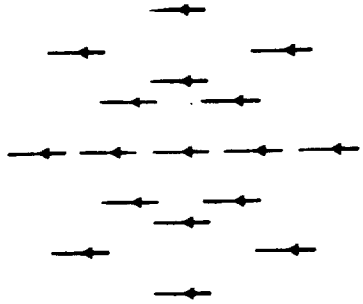

$P_{1200} = j\pi/2$
(d)

Figure 7: Effect of linear retardance aberrations on linearly polarized light. Part (a) shows uniform linearly polarized light in the entrance pupil. Parts (b), (c), and (d) show the polarization state across the exit pupil if the system has only the aberration $P_{1022} = j\pi/2$, $P_{1111} = j\pi/2$, and $P_{1200} = j\pi/2$.

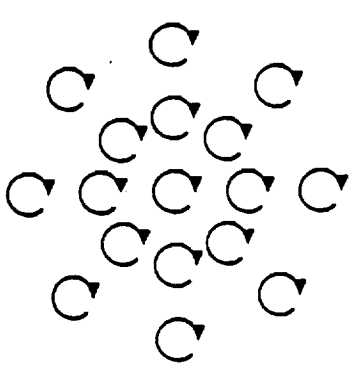

Circularly polarized light incident
(a)

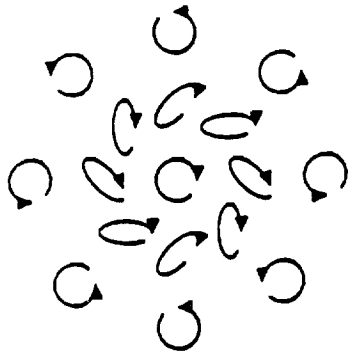

$P_{1022} = j\pi/2$
(b)

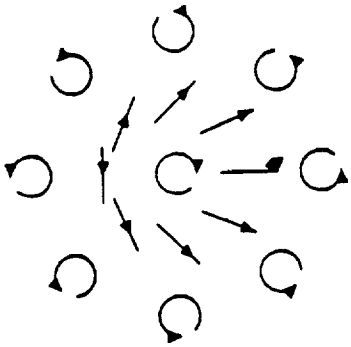

$P_{1111} = j\pi/2$
(c)

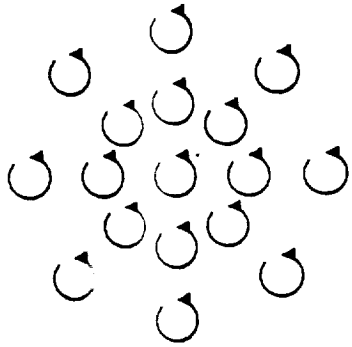

$P_{1200} = j\pi/2$
(d)

Figure 9: Effect of linear retardance aberrations on circularly polarized light. Part (a) shows uniform circularly polarized light in the entrance pupil. Parts (b), (c), and (d) show the polarization state across the exit pupil if the system has only the aberration $P_{1022} = j\pi/2$, $P_{1111} = j\pi/2$, and $P_{1200} = j\pi/2$.

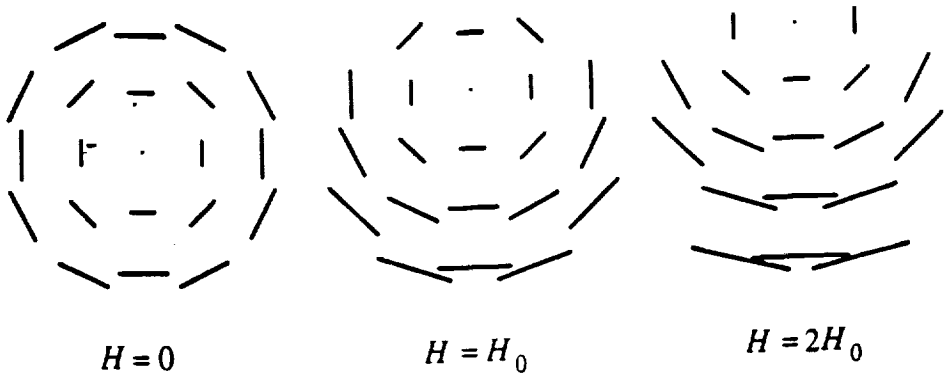

Figure 10: Paraxial angle of incidence at a spherical surface for three field angles. The length of the lines denotes the magnitude of the angle of incidence. The orientation of the lines denotes the orientation of the plane of incidence.

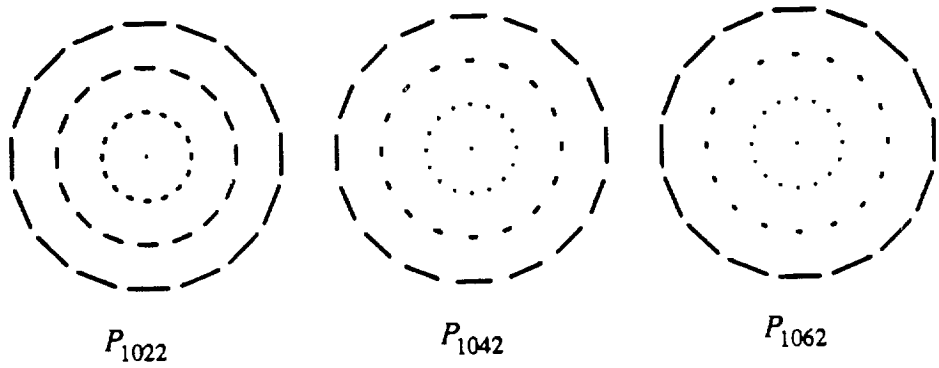

Figure 11: The first three principal vector aberration patterns for isotropic rotationally symmetric interfaces. The P_{1022} pattern varies quadratically with radius. The P_{1042} pattern varies quartically with radius. Finally, the P_{1062} pattern varies with radius to the sixth power.

moves off-axis. The non-principal vector aberration patterns add to the principal pattern to give a decentered view of the principal patterns. The aberrations change as the paraxial angle of incidence function changes for off-axis object points. In fact, the set of nth order vector aberration patterns is complete when the nth order principal pattern can be decentered with a linear combination of the nth order patterns. Again, these principal patterns are analogous to spherical aberration. In classical aberration theory when the object is on-axis, a rotationally symmetric interface only has spherical aberration (but many different orders of spherical aberration). As the object moves off-axis, the other aberrations are introduced.

The completeness of the set of second order vector aberration patterns can be addressed by constructing a shifted second order principal pattern from a linear combination of the second order vector aberrations. Figure 13 shows the second order patterns P_{1022}, P_{1200}, and P_{1111} adding to give a decentered view of the principal pattern. Figure 13 (a) shows the superposition of the P_{1200} and P_{1022} patterns. The vector aberration patterns (arrays of weak linear diattenuators and/or arrays of weak linear retarders) add as PAMs, not as vectors! Two orthogonal weak linear diattenuators of the same magnitude add to zero diattenuation and reduced amplitude (transmission). Two orthogonal weak linear retarders with equal retardance add to zero net retardance. Figure 13 (b) shows the result of adding P_{1200} and

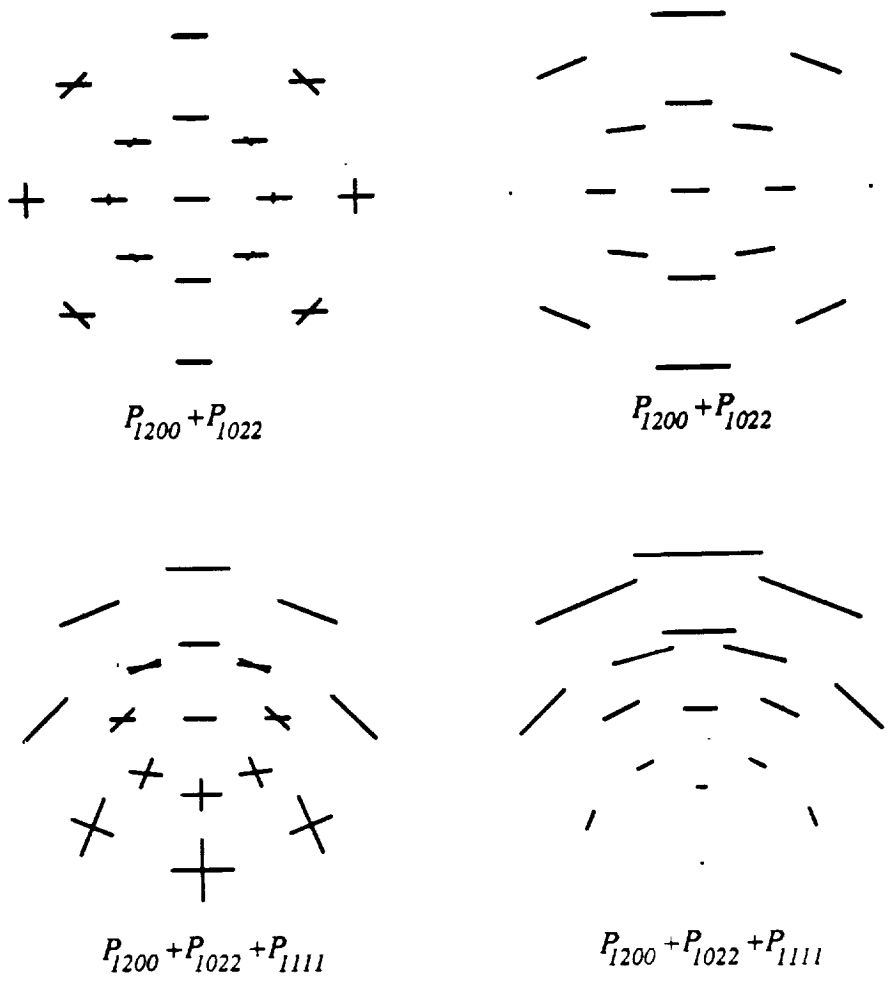

Figure 13: Addition of second order aberration patterns to give a decentered view of the second order principal aberration pattern

Table 6: Symmetry of pupil aberration sections of rotationally symmetric systems

	On Axis Objects	Off Axis Objects	
		Tangential	Sagittal
Aberration type	Linear	Linear	Elliptical
Aberration orientation	Radial or tangential	Horizontal or vertical	Arbitrary
Symmetry	Rotational	None	Odd about the y-axis

Note: An aberration has odd symmetry if the pattern is mirror symmetric about some line.

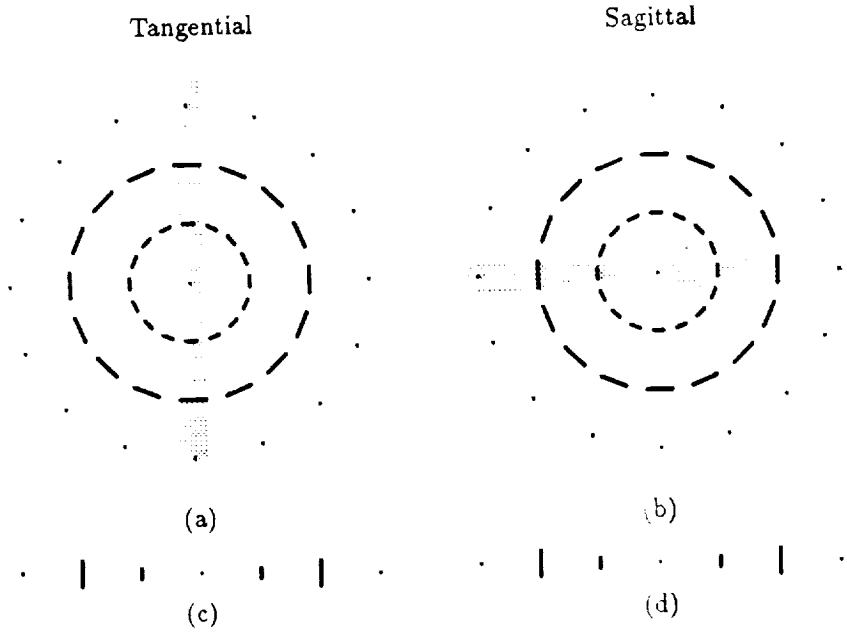

Figure 15: Example pupil aberration section for on axis object. Exit pupil aberration maps with the tangential and sagittal sections highlighted are shown in (a) and (b), respectively. The tangential and sagittal sections are shown in (c) and (d), respectively. The sagittal section is rotated 90 degrees for a more compact display. The aberration is $P_{1022} - P_{1042} + P_{3311}$.

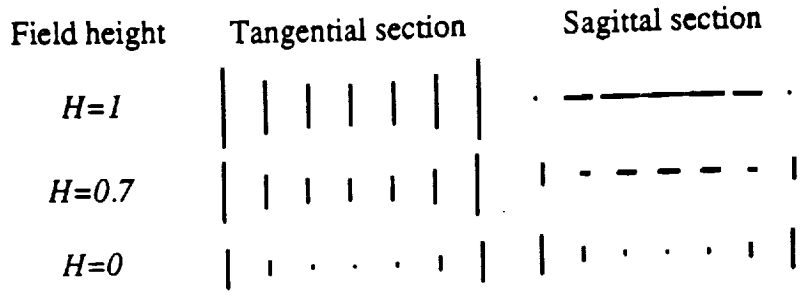

Figure 17: Tangential and sagittal pupil aberrations plot for a system with nth order principal aberrations and piston

can be either diattenuating or retarding giving polarization dependent apodisation or phase, respectively. The circular aberrations described the circular retardance and circular diattenuation introduced by an optical system. For systems of isotropic rotationally symmetric surfaces, the circular aberrations appeared first at fourth order. Vector aberrations were conceptually different from classical aberrations. They described the linear retardance and linear diattenuation variation introduced by an optical system. These polarization aberrations were decomposed into a set of vector patterns which were each attached a weight or an aberration coefficient.

The theory described in this paper applies to many optical systems built today. Thin films have a much deeper role in optical system design than merely changing the transmittance of a system. Thin films induce polarization aberrations or, if the designer is clever, control the polarization aberrations. This extension of aberration theory was made possible by including a Taylor series expansion of the Fresnel coefficients for each interface in the optical system. The resulting aberration theory allows the integration of thin film design and optical design for polarization critical optics.

13 Acknowledgments

The authors wish to acknowledge the support of the Jet Propulsion Laboratory and both the Solar Physics and Optics Branches at Marshall Space Flight Center. Dr. James Breckinridge of the Jet Propulsion Laboratory initially suggested and supported research in the area of instrumental polarization.

A Paraxial Basis Vectors and Fields

In this appendix, we derive the paraxial quantities necessary for the paraxial PAM in Section 6. First, general expressions for the surface normal and local basis vectors are presented. Next, the paraxial approximation is applied to these quantities. The paraxial field is shown to lie in the x-y plane.

where

$$i_{cq} = -\frac{y_{cq}}{R_q} - \frac{r_q \sin u_{cq}}{R_{iq}} \quad \text{(A-11)}$$

$$i_{mq} = -\frac{y_{mq}}{R_q} + \frac{r_q}{R_{iq}} \quad \text{(A-12)}$$

and i_{cq} and i_{mq} are the angle of incidences for the chief and marginal rays respectively. This follows directly from linear nature of the paraxial raytrace [16]. The paraxial system geometry is entirely contained in i_c and i_m. It is not necessary to work with the radii of the individual lenses, entrance pupils, etc. The asphericity and wavefront aberrations have a third order effect on the surface normal and local $(\hat{R}_q, \hat{S}_q, \hat{P}_q)$ basis vectors. Both $\vec{S}_q$ and $\vec{P}_q$ are in the x-y plane. There is no z component of the electric field.

B Polarization at Uncoated Interfaces

This appendix examines the polarization on reflection and transmission from an uncoated interface. We determine the interface coefficients of Chapter 7 with a Taylor series expansion of the Fresnel coefficients. The accuracy is discussed for reflection by gold at $\lambda = 10.6\ \mu$m.

The Fresnel coefficients expanded in the angle of incidence are

$$r_s = \frac{\sin(i-i')}{\sin(i+i')} = \frac{N-1}{N+1}\left(1 - \frac{1}{N}i^2 + \frac{N^2-6N-3}{12N^3}i^4 + \cdots\right) \quad \text{(B-1)}$$

$$r_p = \frac{\tan(i-i')}{\tan(i+i')} = \frac{N-1}{N+1}\left(1 + \frac{1}{N}i^2 + \frac{5N^2-6N+9}{12N^3}i^4 + \cdots\right) \quad \text{(B-2)}$$

$$t_s = \frac{2\cos i \sin(i')}{\sin(i+i')} = \frac{2N}{N+1}\left(1 + \frac{N-1}{2}i^2 + \frac{3N^3+3N^2-7N+1}{24}i^4 + \cdots\right) \quad \text{(B-3)}$$

$$t_p = \frac{\sin(i-i')}{\sin(i+i')} = \frac{2N}{N+1}\left[1 + \frac{N(N-1)}{2}i^2 + \frac{N(N-1)(9N^2-6N+5)}{24}i^4 + \cdots\right] \quad \text{(B-4)}$$

where r_s and r_p are reflection coefficients, t_s and t_p are reflection coefficients, i is the angle of incidence in radians, the $'$ denotes quantities after the interface, $N = n'/n$ is the ratio of the refractive indices, and Snell's law

$$n \sin i = n' \sin i' \quad \text{(B-5)}$$

was used [16,15]. The interface coefficients (B-1) and (B-2) in exponential form are

$$r_s(i) = \exp[r_0 + r_2 i^2 + \cdots] \quad \text{(B-6)}$$

$$r_p(i) = \exp[r_0 - r_2 i^2 + \cdots] \quad \text{(B-7)}$$

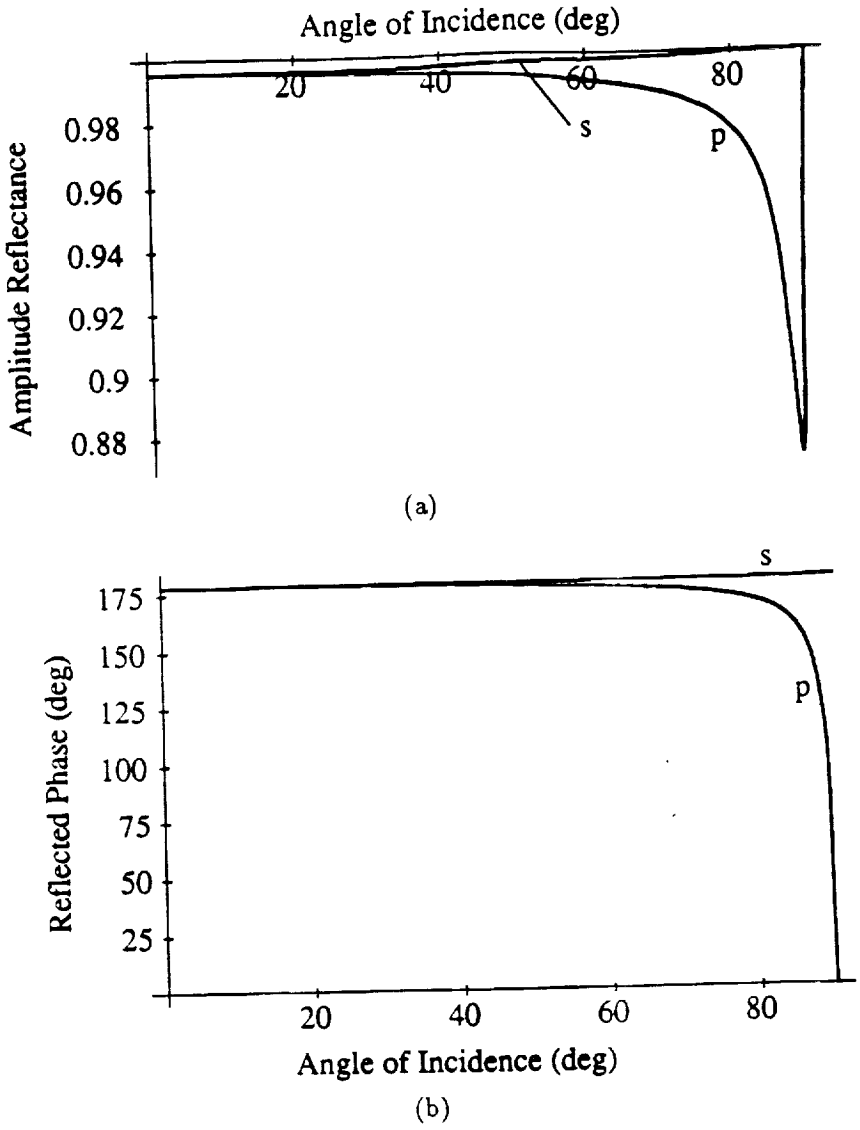

Figure 18: The amplitude reflectance (a) and phase change (b) on reflection from a gold coating at 10.6 μm. Curves are shown for both the s and p components of the incident light. Values were computed using a refractive index, $n = 8.8 - 64j$.

$$P_{0040} = \sum_{q=1}^{Q} a_{04q} i_{mq}^4 \quad \text{(C-9)}$$

$$P_{1200} = \sum_{q=1}^{Q} a_{12q} i_{cq}^2 \quad \text{(C-10)}$$

$$P_{1111} = 2\sum_{q=1}^{Q} a_{12q} i_{cq} i_{mq} \quad \text{(C-11)}$$

$$P_{1022} = \sum_{q=1}^{Q} a_{12q} i_{mq}^2 \quad \text{(C-12)}$$

$$P_{1400} = \sum_{q=1}^{Q} a_{14q} i_{cq}^4 \quad \text{(C-13)}$$

$$P_{1311} = 2\sum_{q=1}^{Q} a_{14q} i_{cq}^3 i_{mq} \quad \text{(C-14)}$$

$$P_{1222} = 3\sum_{q=1}^{Q} a_{14q} i_{cq}^2 i_{mq}^2 \quad \text{(C-15)}$$

$$P_{1133} = 2\sum_{q=1}^{Q} a_{14q} i_{cq} i_{mq}^3 \quad \text{(C-16)}$$

$$P_{1042} = \sum_{q=1}^{Q} a_{14q} i_{mq}^4 \quad \text{(C-17)}$$

$$P_{3131} = j\sum_{q=1}^{Q} \left(a_{12q} i_{mq}^2 \sum_{p=1}^{q-1} a_{12p} i_{cp} i_{mp} - a_{12q} i_{cq} i_{mq} \sum_{p=1}^{q-1} a_{12p} i_{mp}^2 \right) \quad \text{(C-18)}$$

$$P_{3331} = j\sum_{q=1}^{Q} \left(a_{12q} i_{cq} i_{mq} \sum_{p=1}^{q-1} a_{12p} i_{cp}^2 - a_{12q} i_{cq}^2 \sum_{p=1}^{q-1} a_{12p} i_{cp} i_{mp} \right) \quad \text{(C-19)}$$

References

[1] S. Inoué. Studies on depolarization of light at microscope lens surfaces I: The origin of stray light by rotation at lens surfaces. *Exper. Cell Res.*, 3:199–208, 1951.

[2] R. A. Chipman. Polarization analysis of optical systems. *Opt. Eng.*, 28:90–99, 1989.

[3] E. W. Hansen. Overcoming polarization aberrations in microscopy. In R. A. Chipman, editor, *SPIE Proc. 891: Polarization Consideration for Optical Systems*, pages 190–197, SPIE, Bellingham WA, 1988.

[4] R. A. Chipman. Polarization analysis of optical systems. In R. A. Chipman, editor, *SPIE Proc. 1166: Polarization Considerations for Optical Systems II*, SPIE, Bellingham WA, 1989.

[5] J. D. Mangus and J. Alonso. Image sensitivity anomalies of glancing incidence telescopes. In P. W. Sanford, editor, *Proceedings of the X-ray Optics Symposium*, pages 244–275, Mullard Space Sciences Laboratory of University College, London, April 1973.

[23] R. A. Chipman. Polarization raytracing. In C. Londoõn and R. E. Fischer, editors, *SPIE Proc. 766: Recent Trends in Optical System Design; Computer Lens Design Workshop*, pages 61–68, SPIE, Bellingham WA, 1987.

[24] E. Waluschka. Polarization ray trace. *Opt. Eng.*, 28:86–89, 1989.

[25] J. Sánchez Mandragón and K. B. Wolf, editors. *Lie Methods in Optics. Lecture Notes in Physics*, Springer-Verlag, Berlin, 1986.

[26] P. Jacquinot and Mme B. Roizen-Dossier. Apodisation. In E. Wolf, editor, *Progress in Optics*, North Holland, Amsterdam, 1964.

[27] C. Whitney. Pauli-algebraic operators in polarization optics. *J. Opt. Soc. Am.*, 61:1207–1213, 1971.

Polarization aberrations. II. Tilted and decentered optical systems

James P. McGuire Jr.
Russell A. Chipman

May 21, 1990

Many optical systems built have tilted or decentered elements. These include unobscured systems and systems with fold flats. Because of typically larger angles of incidence, polarization aberrations can be significant in these systems. Two types of tilted and decentered systems composed of rotationally symmetric elements are examined. One is systems with collinear centers of curvatures but with decentered pupils. Symmetry in such systems allows the analysis to proceed along lines very similar to those in Paper I. The other is systems with arbitrary tilts and decenters. In these systems, the field dependences of the aberrations from each surface are not concentric. The extension is made by using a polarization aberration matrix with vector, instead of scalar, arguments.

The extension to tilted and decentered systems used in this paper is based on the principle that each surface has an axis of symmetry; and these aberrations can be found in the conventional fashion. Buchroeder used this principle to design systems composed of tilted and decentered elements [1]. Thompson used vector algebra to combine the aberration contributions from tilted and decentered elements [2]. Rogers extended the vector techniques to explore anamorphic and keystone distortion due to the tilt of the object relative to the elements in the optical system [3].

Section 1 briefly introduces the basis of aberration theory for tilted and decentered systems. Section 2 outlines the coordinate system and some vector operations. In Section 3 we present the PAM with vector arguments which is the basis of the calculations in this paper. Section 4 examines systems with decentered pupils. Example calculations for an infrared LIDAR beam expander are given in Section 5. Section 6 explores aberrations in systems with arbitrary tilts and decenters. The second order PAM of Section 3 is manipulated into a form convenient for summing a system of tilted and decentered elements. The accuracy of this method is discussed. A simple IR scan mirror assembly is analyzed in Section 7. References to equations and sections in Paper I are preceded I.

1 Overview

Each spherical surface and its entrance pupil form a rotationally symmetric system. Thus, each optical surface introduces aberrations of the same form, whether used in a rotationally symmetric or unsymmetric system. The centers of the aberration contributions of each surface are displaced due to the tilt. Figure 1 shows a spherical surface, pupil, and object. The axis of symmetry is called the *local axis* and connects the center of the pupil and the center of curvature for the surface. The *central ray* is defined by the center of the object and the center of the pupil for the surface. Both the object field and the pupils for each surface are found by imaging the object and the entrance pupil through each of the surfaces prior to the surface in question. In rotationally symmetric systems, the local axis and the central ray coincide. In systems with decentered pupils, the vector aberration expansion is made about the line connecting the centers of curvatures of the elements. In arbitrarily tilted and decentered systems, the vector aberration expansion for tilted optical systems is made about the local axis of each element.

When the center of the pupil coincides, or nearly coincides, with the center of curvature of the mirror (i.e. in a *Schmidt* system), the local axis is either ill-defined or so oblique that aberration expansions about it are impractical. In these cases, the expansion should be made about the line connecting the object and the center of curvature. The optical system is rotationally symmetric about this line with the pupil decentered and tilted instead of the object.

$$\begin{aligned} \vec{\rho} &= (\rho, \phi) \\ &= \rho_x \hat{x} + \rho_y \hat{y} \end{aligned} \tag{3}$$

where ρ and ϕ are the polar pupil coordinates. The pupil vector is normalized so that $\rho = 1$ at the edge of a circular pupil.

Vector multiplication introduced by Thompson [2] is analogous to complex number multiplication

$$\vec{H}\vec{\rho} = (H\rho, \theta + \phi) \tag{4}$$

and gives a vector result. The square root of a vector

$$\sqrt{\vec{H}} = \left(\sqrt{H}, \frac{\theta}{2}\right) \text{ or } \left(\sqrt{H}, \frac{\theta}{2} + \pi\right) \tag{5}$$

is a vector and follows directly from the definition of vector multiplication. The dot product

$$\begin{aligned} \vec{H} \cdot \vec{\rho} &= H_x \rho_x + H_y \rho_y \\ &= H\rho\cos\phi \end{aligned} \tag{6}$$

gives a scalar result. The following vector identities

$$2\left(\vec{A}\cdot\vec{B}\right)\left(\vec{A}^2\cdot\vec{C}^2\right) = A^2\left(\vec{A}\vec{B}\cdot\vec{C}^2\right) + \left(\vec{A}^3\cdot\vec{B}\vec{C}^2\right) \tag{7}$$

$$2\left(\vec{A}\cdot\vec{B}\right)\left(\vec{A}\cdot\vec{C}\right) = \left(\vec{A}^2\cdot\vec{B}\vec{C}\right) + A^2\left(\vec{B}\cdot\vec{C}\right) \tag{8}$$

$$2\left(\vec{A}\cdot\vec{B}\right)\left(\vec{A}\vec{B}\cdot\vec{C}^2\right) = A^2\left(\vec{B}^2\cdot\vec{C}^2\right) + B^2\left(\vec{A}^2\cdot\vec{C}^2\right) \tag{9}$$

are useful in the manipulation of vector aberrations. All are easily verified by converting to trigonometric form.

3 Polarization Aberration Matrices with Vector Arguments

In this section, we discuss PAMs for a single surface with vector arguments. The PAM with scalar arguments is rewritten first for arbitrary object orientations and then with vector notation.

First consider the second order terms in the PAM derived in Section I.9

$$\mathbf{J}(H,\rho,\phi) = \exp\left\{\begin{array}{ll} P_{0000}\boldsymbol{\sigma}_0 + & \text{constant piston} \\ P_{0200}H^2\boldsymbol{\sigma}_0 + & \text{quadratic piston} \\ P_{0111}H\rho\cos\phi\,\boldsymbol{\sigma}_0 + & \text{tilt} \\ P_{0020}\rho^2\boldsymbol{\sigma}_0 + & \text{defocus} \\ P_{1200}H^2\boldsymbol{\sigma}_1 + & \\ P_{1111}H\rho(\cos\phi\,\boldsymbol{\sigma}_1 - \sin\phi\,\boldsymbol{\sigma}_2) + & \\ P_{1022}\rho^2(\cos 2\phi\,\boldsymbol{\sigma}_1 - \sin 2\phi\,\boldsymbol{\sigma}_2) & \end{array}\right\} \tag{10}$$

Equation (10) describes the aberrations for objects of height H located along the y-axis. The pupil dependence is described by polar coordinates (ρ, ϕ) with ϕ measured from the object (which lies on the y-axis). If the object is located θ from the y-axis, then the PAM is

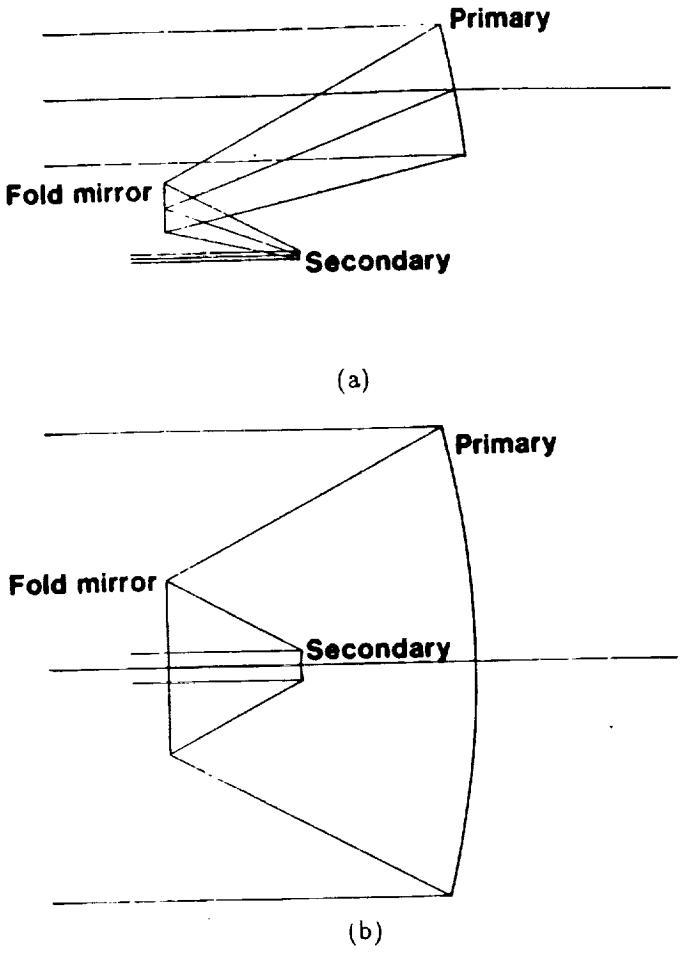

Figure 3: IR LIDAR off-axis beam expander (a) and the equivalent rotationally symmetric system (b). In systems with decentered pupils such as (a), the aberrations are easily calculated by analyzing the equivalent rotationally symmetric system (b) and then decentering the pupil.

Table 1: Optical design of the LIDAR off-axis beam expander and the associated chief and marginal angles of incidence

Overall	
F-number	1
Expansion ratio	16:1
Field of view	50 μrad
Diameter	110 cm
Coatings	Gold
Wavelength	10.6 μm
Parabolic primary	
Focal length	110 cm
Diameter	110 cm
Off axis section diameter	30 cm
Beam displacement from optical axis	50 cm
Parabolic secondary	
Focal length	6.875 cm
Diameter	7.5 cm
Beam displacement from optical axis	2.5 cm
Paraxial angles of incidence	
Chief	
At primary mirror (i_{c1})	-50 μrad
At fold mirror (i_{c2})	50 μrad
At secondary mirror (i_{c3})	424 μrad
Marginal	
At primary mirror (i_{m1})	750 mrad
At fold mirror (i_{m2})	-500 mrad
At secondary mirror (i_{m3})	72.7 mrad

Table 2: Aberration coefficients for the LIDAR beam expander

$P_{0000} = -0.012 - 0.092j$
$P_{0200} = 0$
$P_{0111} = 0$
$P_{0020} = 0$
$P_{1200} = 3.5 \times 10^{-10} + 2.8 \times 10^{-9}j$
$P_{1111} = -1.8 \times 10^{-7} - 1.4 \times 10^{-6}j$
$P_{1022} = 0.002 + 0.013j$

$$\mathbf{J}\left(\vec{H},\vec{\rho}\right) = \exp\left\{\begin{array}{ll} \sum_q P_{0000q}\sigma_0 + & \text{constant piston} \\ \sum_q P_{0200q}\left(\vec{H}-\vec{h}_q\right)\cdot\left(\vec{H}-\vec{h}_q\right)\sigma_0 + & \text{quadratic piston} \\ \sum_q P_{0111q}\left(\vec{H}-\vec{h}_q\right)\cdot\vec{\rho}\,\sigma_0 + & \text{tilt} \\ \sum_q P_{0020q}\vec{\rho}\cdot\vec{\rho}\,\sigma_0 + & \text{defocus} \\ \sum_q P_{1200q}\left(\vec{H}-\vec{h}_q\right)^2\cdot\vec{A} + & \\ \sum_q P_{1111q}\left(\vec{H}-\vec{h}_q\right)\vec{\rho}\cdot\vec{A} + & \\ \sum_q P_{1022q}\vec{\rho}^{\,2}\cdot\vec{A} & \end{array}\right\} \tag{15}$$

which may be rewritten

$$\mathbf{J}\left(\vec{H},\vec{\rho}\right) = \exp\left\{\begin{array}{l} P_{1200}\left[\left(\vec{H}-\vec{a}_{1200}\right)^2 - \vec{b}_{1200}^2\right]\cdot\vec{A} + \\ P_{1111}\left(\vec{H}-\vec{a}_{1111}\right)\vec{\rho}\cdot\vec{A} + \\ P_{1022}\vec{\rho}^{\,2}\cdot\vec{A} \end{array}\right\} \tag{16}$$

where the polarization independent aberrations P_{0uvw} were dropped and the aberration coefficients are

$$P_{1200} = \sum_q P_{1200q} \tag{17}$$

$$\vec{a}_{1200} = \frac{1}{P_{1200}}\sum_q P_{1200q}\vec{h}_q \tag{18}$$

$$\vec{b}_{1200}^2 = \vec{a}_{1200}^2 - \frac{1}{P_{1200}}\sum_q P_{1200q}\vec{h}_q^2 \tag{19}$$

$$P_{1111} = \sum_q P_{1111q} \tag{20}$$

$$\vec{a}_{1111} = \frac{1}{P_{1111}}\sum_q P_{1111q}\vec{h}_q \tag{21}$$

$$P_{1022} = \sum_q P_{1022q} \tag{22}$$

Equation (16) describes the polarization dependent aberrations through second order for systems of tilted and decentered elements. The interpretation of each aberration is discussed below.

The first aberration to consider is *polarization defocus*

$$P_{1022}\vec{\rho}^{\,2}\cdot\vec{A} \tag{23}$$

Since each contribution to the defocus terms is independent of $\vec{H}$ and therefore $\vec{h}$, the aberration is independent of the tilts or decenters of the elements.

The next term to consider is *polarization tilt*

$$P_{1111}\left(\vec{H}-\vec{a}_{1111}\right)\vec{\rho}\cdot\vec{A} \tag{24}$$

which shows the aberration resulting from a sum of tilts is of the same form as a single surface tilt. Figure 6 shows the pupil aberration for the tilt aberration in (a) rotationally symmetric system and (b) tilted and decentered system. The aberration is centered in the field at $\vec{a}_{1111}$. The strength of the aberration is given

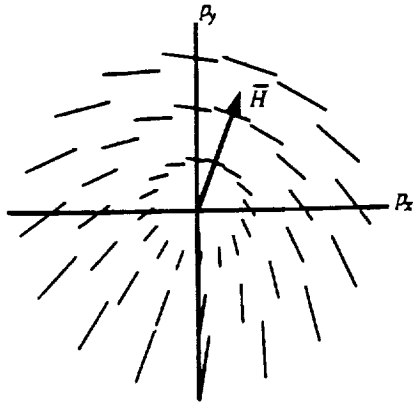

(a)

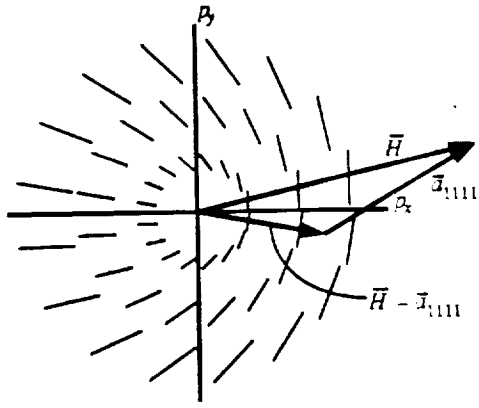

(b)

Figure 6: The pupil aberration map for the tilt aberration. Examples for (a) rotationally symmetric systems and (b) tilted or decentered systems are shown. The object vectors are superimposed over the pupil to show the effect of the tilts and decenters on the orientation of the aberration pattern.

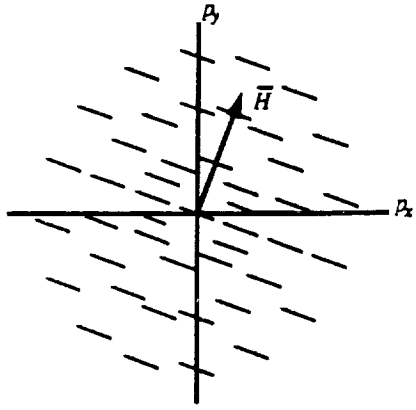

(a)

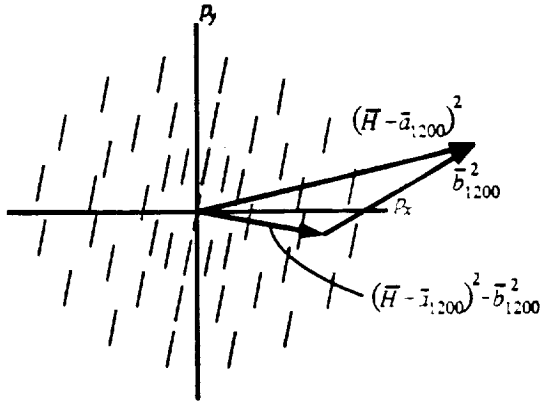

(b)

Figure 8: The pupil aberration map for quadratic piston aberration. Examples for (a) rotationally symmetric systems and (b) tilted or decentered systems are shown. The object vectors are superimposed over the pupil to show the effect of the tilts and decenters on the orientation of the aberration pattern.

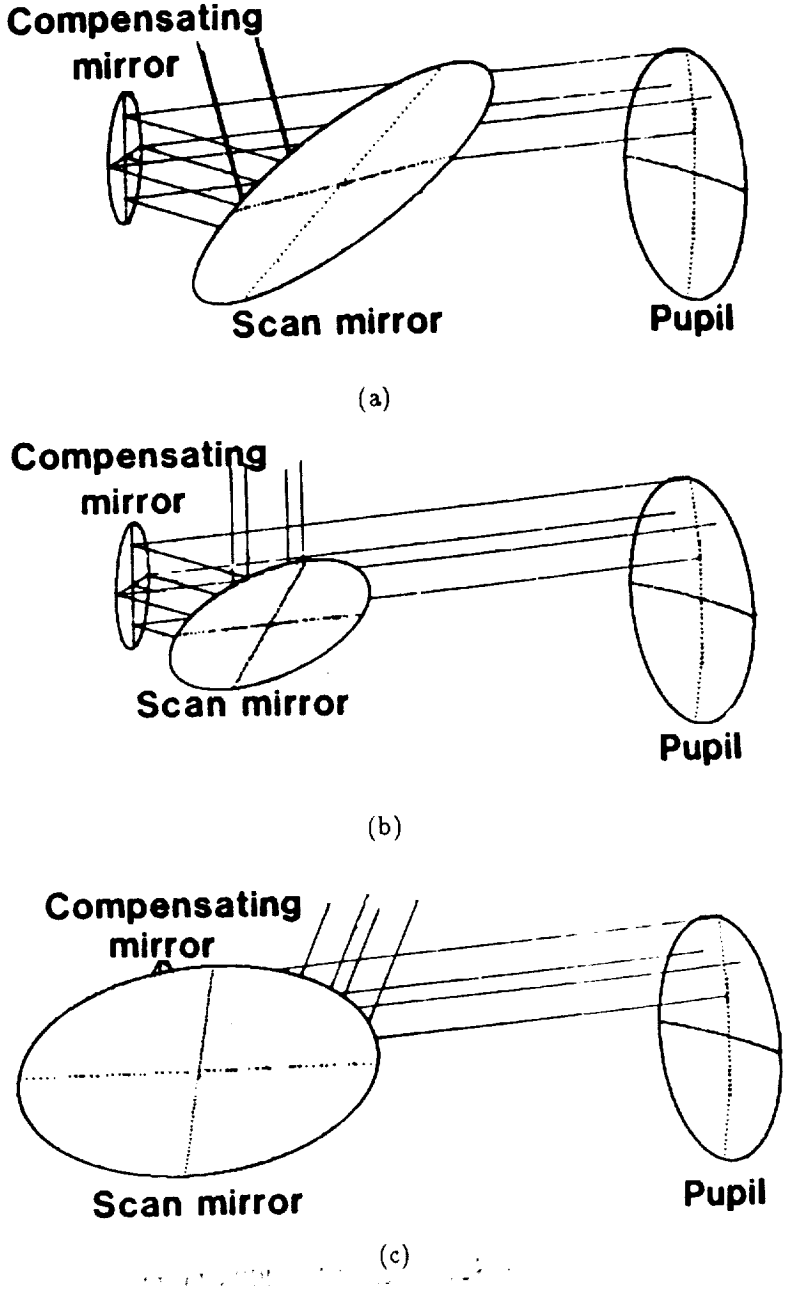

Figure 10: Infrared scan mirror system pointed at (a) 22.5°, (b) 45°, and (c) 67.5°. The fixed pupil of the optical system is shown.

Polarization Analysis of LIDARs

Dr. James P. McGuire, Jr. Dr. Russell A. Chipman
Physics Department
University of Alabama in Huntsville
Huntsville, Alabama 35899

June 8, 1990

1 Introduction

The objective of LIDAR systems is to accurately measure atmospheric winds. The measurement proceeds as follows. A circularly polarized beam is sent by the LIDAR into the atmosphere. Particulates backscatter some of the light back into the LIDAR and change the handedness of the circularly polarized light. The return signal is combined with the local oscillator at the heterodyne receiver using a polarizing beamsplitter. Doppler shifts and trip time of the return beam provide velocity and ranging information.

Any difference in the polarization state of the return beam from the expected circular polarization state, decreases the fraction of the return signal combined with the local oscillator. Thus changes in polarization due to the optics before the beamsplitter, reduce signal and instrumental accuracy. This loss of signal due to instrumental polarization can be minimized during the design phase, if polarization is understood.

All of the mirrors in LIDAR systems change the polarization state of the light because the rays strike at non-normal incidence. The polarization change depends on field position, object position, and incident polarization state. Polarization aberrations couple some portion of the incident polarization state into the orthogonal polarization state. Polarization analysis of optical systems is reviewed by Chipman[1].

2 Results

Significant contributions in two areas of polarization analysis were made: aberration theory and polarization raytracing. The results are described in two papers which were completed with funding from this contract[2,3] and have been submitted to *Optical Engineering* for publication. These papers are the final report for this contract. This contract also provided partial support for the completion of Dr. McGuire's dissertation [4]. Some important aspects of this research are highlighted below.

Polarization aberration theory describes the low order polarization in an optical system with a Taylor series approximation. This approximation is particularly good in reflective IR systems because of the high indices of IR materials. Section II.5 uses polarization aberration theory to analyze a NASA IR LIDAR beam-expander. Polarization aberrations were found to couple less than 1.0% of the light into the orthogonal polarization state.

Polarization raytracing is the analogue of conventional raytracing with the polarization modifying properties of the system calculated instead of optical path differences. Current commercial polarization raytracing codes [5,6] are good at cal-

culating the polarization of an optical system. However the results are not presented in a form which leads to a thorough understanding of the polarization aberrations in a system. Section I.8 discusses several alternative methods of display which would make the design of LIDAR or any polarization critical system far easier. Discussions about incorporatating these new techniques have been initiated with lens design software developers. Improved polarization analysis software should result.

References

[1] R. A. Chipman. Polarization analysis of optical systems. *Opt. Eng.*, 28:90–99, 1989.

[2] J. P. McGuire, Jr. and R. A. Chipman. Polarization aberrations in optical systems. In R. E. Fisher and W. J. Smith, editors, *SPIE Proc. 818: Current Developments in Optical Engineering II*, pages 240–257, SPIE, Bellingham WA, 1987. A revised version of this paper, "Polarization aberrations. I. Rotationally symmetric optical systems," including exponential form and several other refinements has been submitted to *Opt. Eng.* 1990.

[3] J. P. McGuire, Jr. and R. A. Chipman. Polarization aberrations. II. Tilted and decentered optical systems. 1990. This paper has been submitted to *Opt. Eng.*

[4] J. P. McGuire, Jr. *Image formation and analysis in optical systems with polarization aberrations.* PhD thesis, University of Alabama in Huntsville, 1990.

[5] *CODE V.* Optical Research Associates, Pasadena CA, 1989.

[6] *SYNOPSYS.* Eastboothbay MA, 1988.

003464
Pg. 32

NASA
National Aeronautics and Space Administration

Report Documentation Page

1. Report No. Final Draft	2. Government Accession No.	3. Recipient's Catalog No.
4. Title and Subtitle Polarization Effects (Tasks 1 & 2)		5. Report Date 8/16/90 6. Performing Organization Code 5-32186
7. Author(s) McGuire/Chipman		8. Performing Organization Report No. Draft Final 10. Work Unit No.
9. Performing Organization Name and Address University of Alabama in Huntsville Center for Applied Optics Huntsville, AL 35899		11. Contract or Grant No. NAS8-36955, D.O. 33 13. Type of Report and Period Covered Final Draft
12. Sponsoring Agency Name and Address NASA/MSFC		14. Sponsoring Agency Code EB-23

15. Supplementary Notes

16. Abstract

17. Key Words (Suggested by Author(s))	18. Distribution Statement		
19. Security Classif. (of this report)	20. Security Classif. (of this page)	21. No. of pages	22. Price

NASA FORM 1626 OCT 86